Alexander, P., Schmidt, T., de la Torre, A. (2018): A Method to Determine Gravity Wave Net Momentum Flux, Propagation Direction, and “Real” Wavelengths: A GPS Radio Occultations Soundings Case Study. - *Earth and Space Science*, *5*, 6, pp. 222—230.

DOI: http://doi.org/10.1002/2017EA000342

AGU100 ADVANCING EARTH AND SPACE SCIENCE

Earth and Space Science

RESEARCH ARTICLE
10.1002/2017EA000342

Special Section:
Planetary Mapping: Methods, Tools for Scientific Analysis and Exploration

A Method to Determine Gravity Wave Net Momentum Flux, Propagation Direction, and "Real" Wavelengths: A GPS Radio Occultations Soundings Case Study

P. Alexander[1], **T. Schmidt**[2], **and A. de la Torre**[3]

[1]Instituto de Física de Buenos Aires, CONICET, Ciudad Universitaria Pabellón 1, Buenos Aires, Argentina, [2]Helmholtz Centre Potsdam, GFZ German Research Centre for Geosciences, Potsdam, Germany, [3]LIDTUA, Facultad de Ingeniería, Universidad Austral and CONICET, Buenos Aires, Argentina

Key Points:
- Previous GW parameters solution schemes are modified for the use of close sounding quartets
- The method calculates GW propagation direction, net MF, and "real" (not apparent) vertical wavelength
- The future increase of soundings may lead to GW climatologies of the above parameters by this method

Correspondence to:
P. Alexander,
peter@df.uba.ar

Citation:
Alexander P., Schmidt T., & de la Torre, A. (2018). A method to determine gravity wave net momentum flux, propagation direction, and "real" wavelengths: A GPS radio occultations soundings case study. *Earth and Space Science*, *5*, 222–230. https://doi.org/10.1002/2017EA000342

Received 6 OCT 2017
Accepted 22 MAR 2018
Accepted article online 10 MAY 2018
Published online 15 JUN 2018

Abstract Atmospheric gravity waves (GW) serve as an essential mechanism in the transport of energy and momentum flux from the low to the upper atmosphere. In the last decades satellite observations have become an important part in the analysis of GW due to their global and frequent coverage. Present procedures often provide GW absolute momentum flux (MF), ambiguous 3-D propagation direction, and apparent vertical wavelengths. We here introduce a method with close sounding quartets, which allows the calculation for GW of the net MF, the definite propagation direction, and "real" wavelengths. Among the satellite observational techniques, Global Positioning System (GPS) radio occultation (RO) retrievals provide temperature profiles that after adequate processing may yield GW properties like wavelengths, MF, and energy. Our procedure is illustrated by an example under requirements that tend to ensure that four GPS RO soundings are observing the same GW. The future increase of satellite measuring devices due to new missions (including GPS RO) will lead to a higher spatial and temporal density of profiles that may eventually allow the attainment of GW climatologies of net MF, propagation direction, and "real" vertical wavelengths.

1. Introduction

Gravity waves (GW) are mostly generated in the troposphere and are very important in controlling the dynamics of the stratosphere and upper layers. The major GW influences occur in the middle atmosphere (up to about 100 km) because of the increasing wave amplitudes with altitude. Diverse studies (e.g., P. Alexander, de la Torre, Schmidt, et al., 2015) have indicated a potential for GW penetration into the termosphere and ionosphere, where other physical mechanisms become dominant. The momentum flux (MF) and energy that they carry from the lower to the middle and upper atmosphere play a crucial role from mesoscale to global scales. In particular, as climate simulations do not resolve the full spectrum of GW and as observational constraints for them are scarce, their effect has to be represented within the numerical models by drag parameterizations based on simple physical assumptions. The chosen representations govern the resulting profile of simulated MF, which is relevant in the knowledge of the GW breaking levels, the vertical dissipation characteristics and the forcing on the mean flow. Model tuning parameters are used to modify this flux in order to obtain realistic middle atmosphere winds and temperatures. Nevertheless, biases are observed and they are attributed to these parameterizations being deficient. This fact urges for observational information on GW sources, their propagation, breaking, and diffusion and their spatial and temporal variability (e.g., Geller et al., 2013; Plougonven & Zhang, 2014).

Some decades ago the observational information of GW was provided by measurements from the ground or in situ like rockets, aircrafts, radars, lidars or radiosondes. These platforms provided data only at specific geographical locations and under appropriate meteorological conditions. However, the ample need for GW observations required a continuous attainment of data on global scales. The accomplishment of this aim has only been possible in the satellite era, mainly with an increasing amount of profiles in the last two decades. However, satellite-based retrievals also have their pitfalls. At present, two difficulties of the satellite profiles and their afterward processing methods regarding the study of GW (M. J. Alexander, Gille, et al., 2008; P. Alexander, de la Torre, & Llamedo, 2008; Ern et al., 2004; Preusse et al., 2002) are as follows: (a) There is a need for the determination of the net momentum flux, but usually absolute values are obtained and in addition a

wave propagation direction ambiguity cannot be elucidated, and (b) there always is a discrepancy between "real" (from hereon just real) wavelengths and apparent (measured) ones. Specifically, unless measuring trajectories exhibit configurations that are perfectly parallel or perpendicular to the ground, observed horizontal and vertical wavelengths will differ from real ones. Regarding the discrepancy between apparent and real horizontal wavelengths, the problem has already been satisfactorily addressed in previous work (e.g., Ern et al., 2004; Faber et al., 2013; Wang & Alexander, 2010).

A direct measurement with satellites of absolute GW MF, propagation direction, and real wavelengths is in general not possible. Just one sounding cannot provide enough information to infer them, but they can all be deduced with additional retrievals through the phase shift between GW-induced perturbations on close temperature profiles and the knowledge of their spatial and temporal separation. M. J. Alexander (2015) stressed the relevance of adequately studying the time and three-dimensional structure of GW, Wright et al. (2016) highlighted the importance of obtaining net rather than absolute GW MF calculations, de la Torre et al. (2018) quantified the possible dramatic differences between apparent and real wavelengths and the corresponding significant effects on the calculation of derived GW parameters, whereas Ern et al. (2017) derived net GW MF from temperature data of a nadir-viewing satellite instrument.

In the present study we employ for the first time a set of four close (in space and time) atmospheric soundings in order to infer the ground-based frequency and the zonal, meridional, and vertical real wavelengths of a dominant GW in a sounded region. Some previous GW MF studies focused on triples to find the two real horizontal wavelengths. Usually, they calculated the absolute MF and determined an ambiguous GW propagation direction. In some studies apparent and real vertical wavelengths were wrongly taken as equivalent. Our method below allows to determine without sign ambiguities the three phase velocity components (i.e., the wave propagation direction or phase progression), the net GW MF, and the three real wavelengths. Section 2 explains the analysis procedure allowing to find out the ground-based GW frequency, the three real wavelengths, and thereafter the propagation direction and the net MF and elaborate comparisons between real and apparent vertical wavelengths. It also gives an overview and specifications of the Global Positioning System (GPS) radio occultation (RO) observations that we use for application of our method and exhibits some details of these retrievals. Section 3 presents an application example, and section 4 summarizes the main results of our case study and the possible benefits of the future application of the method.

2. Data and Method

GPS RO is a unique satellite technique regarding the retrieval of global and continuous (but nonuniform in space and time) atmospheric information, which is not affected by meteorological conditions. It presently provides about 2,000 daily profiles of water vapor, temperature, refractivity, and pressure from the troposphere up to the middle stratosphere. In April 2006, the Constellation Observing System for Meteorology, Ionosphere, and Climate (COSMIC) mission launched six GPS RO satellites, which significantly increased the number of daily available profiles at that time. For some months after the COSMIC launch all of its satellites were nearly together and there were several sets of close in space and time soundings, but thereafter the orbit characteristics changed and the amount of this kind of sets decreased significantly. The present study analyzed all the newest so-called reprocessed data from all available RO missions (CHAMP, SAC-C, GRACE, etc.) provided by CDAAC (COSMIC Data Analysis and Archive Center), but we only found sets of adequately close profiles during the early months of the COSMIC mission.

GPS RO is a limb sounding method that has an observational window that allows it to detect only a portion of the GW spectrum (as all other techniques). It is particularly sensitive to GW with small ratios of vertical to horizontal wavelengths (Wu et al., 2006). Its vertical and horizontal resolutions are respectively around 1 and 200 km (Kursinski et al., 1997). Lange and Jacobi (2003) concluded that horizontal wavelengths smaller than about 100 km will hardly leave any imprint on the retrievals, whereas Marquardt and Healy (2005) found out that only vertical wavelengths above 2 km may be observed. The so-called RO dry temperature profiles reflect air temperature usually above 10 km height (where moisture is negligible), but they are not reliable for extracting GW above 30 km (Luna et al., 2013). We therefore consider the height interval 10 to 30 km for calculations, which roughly coincides with the altitudes where RO profiles are the result of a high amount of observational component with respect to background information (Healy & Eyre, 2000).

A first step requires the separation in the T profiles of GW from the background (including planetary waves). Special care has to be taken in avoiding spurious amplifications of GW near the tropopause, which usually

occur after the use of a digital filter to isolate them (de la Torre et al., 2006). It must be also considered that different isolation methods may lead to diverse GW results (John & Kumar, 2013). According to the conclusions of Schmidt et al. (2016) we regard the use of ERA Interim reanalysis data as the most reliable method for obtaining the background temperature, which was here prepared in daily 10° by 5° longitude latitude bins. Ideally, after this separation procedure the remaining perturbation profiles contain only contributions from GW.

Following previous approaches (e.g., Ern et al., 2004; Faber et al., 2013; Schmidt et al., 2016), we assume that one dominant monochromatic GW exists in each analyzed case, whose parameters become determined. The perturbed temperature T' may be then represented by

$$T'(x, y, z, t) = To(z)\sin(kx + ly + mz - \omega t + \varphi_0) \tag{1}$$

where x, y, z, and t represent horizontal and vertical coordinates and time; k, l, m, and ω are the corresponding wave numbers and frequency as seen from the ground; To is the GW amplitude; φ_0 is a constant and the whole expression within parentheses on the right is called the wave phase. Observations will be here evaluated in equation (1) at the vertical but slanted profile positions. Between two diverse times and positions i and j the phase differences $d\phi_{ij}$ are given by

$$d\phi_{ij} = k(x_i - x_j) + l(y_i - y_j) + m(z_i - z_j) - \omega(t_i - t_j) \tag{2}$$

Close triples have already been used to infer $|\ k\ |$ and $|\ l\ |$ (e.g., Ern et al., 2004; Schmidt et al., 2016): Phase differences are calculated from two profiles with respect to the remaining one at constant height and with negligible time difference. Therefore, two linear equations provide the two wavelength components at each constant height. A fourth sounding should be added with nonnegligible time difference with respect to the other ones to also obtain ω, leading to three equations with three unknowns. In order to also incorporate m we will not include another retrieval, but we will use one of the already existing ones at two different heights (see the complete configuration in Figure 1). Our equation system will look like this at every altitude z_1 (13.1, 13.2, ..., 27.0 km; a solution for the complete 10-30 km height range cannot be obtained as explained below)

$$d\phi_{21} = k(x_2 - x_1) + l(y_2 - y_1) \tag{3}$$

$$d\phi_{31} = k(x_3 - x_1) + l(y_3 - y_1) \tag{4}$$

$$d\phi_{41} = k(x_4 - x_1) + l(y_4 - y_1) - \omega(t_4 - t_1) \tag{5}$$

$$d\phi_{1^*1} = k(x_1^* - x_1) + l(y_1^* - y_1) + m(z_1^* - z_1) \tag{6}$$

where 1^* means that profile 1 becomes evaluated at height z_1^* instead of z_1 (and also at x_1^*, y_1^* instead of x_1, y_1). The four equations contain four unknowns (k, l, m, ω), whereas the four phase differences may be inferred as explained below and the 12 coordinate differences may be easily calculated from the available RO information. At every height level z_1 then k, l, m, ω are simultaneously obtained by a standard linear equation set solution procedure, so we obtain the three wavelength components and the frequency as a function of altitude. The use of the time difference in equation (5) is the key to find net rather than absolute GW phase progression and MF values. If it was not introduced, then the equation system would be like a static photo where no motion information was introduced into the description of the scenario. Another slightly modified version of the above equation set would have two pairs, each one containing nearly simultaneous RO, but each pair separated from the other by a nonnegligible time. However, we found no quartets like this option. Equations (3)–(4) are the same as used, for example, by Schmidt et al. (2016) for close in time triples. In equation (6) $z_1^* - z_1$ will be 3 km, which is about twice the lowest vertical resolution of RO, that is, 1.4 km in the stratosphere (Kursinski et al., 1997). Notice that whereas equation (6) in combination with (3)–(5) senses the real vertical wavelength, an identification with the apparent value from a T' versus z representation from a single RO is wrong, as this sounding is not perfectly vertical. Therefore, one should be extremely cautious on the requirement (in previous works) for small differences between apparent vertical wavelengths from close RO in order to obtain acceptable GW MF calculations. Here we will alternately use the three remaining RO in equation (6) and compare the four real vertical wavelength results among them in order to decide wether the same GW was likely present along the four ROs. McDonald (2012) evaluated as a function of horizontal separation and time difference the percentage of paired profiles that may be expected to contain the same GW.

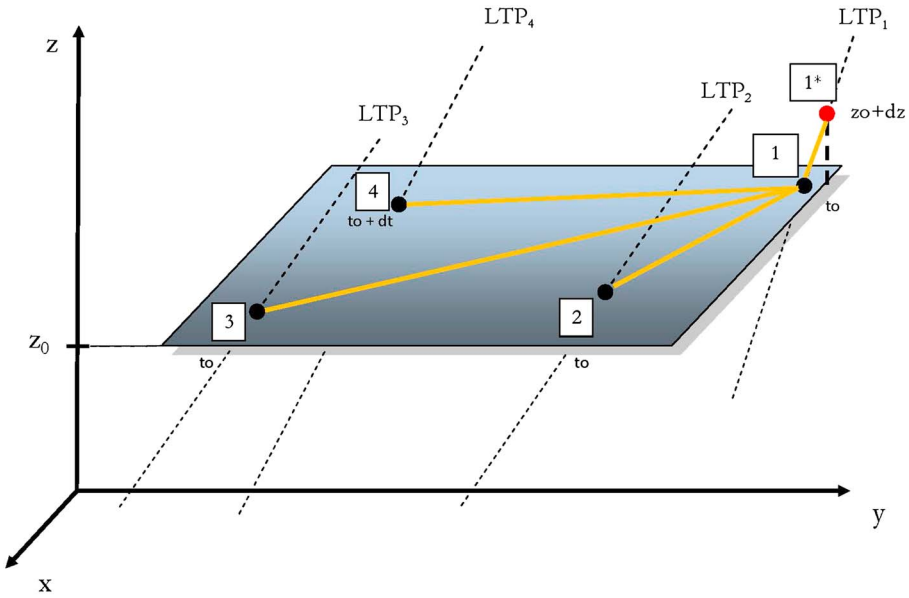

Time difference dt between profiles 4 and 1 is calculated. The procedure will start at 13 km height.
1. Coordinate differences between profiles 4, 3, 2 with respect to 1 are obtained.
2. Phase differences between profiles 4, 3, 2 with respect to 1 are obtained.
3. Horizontal coordinate differences between positions at zo and at zo + dz in profile 1 are calculated.
4. Phase difference between zo and zo + dz in profile 1 is calculated.
5. System solution leads to frequency and the three wavelength components at the present height level.
6. Increase height level by 0.1 km and go to 1 until height 27 km is reached.

Figure 1. An illustration of the quartet configuration showing the line of tangent points (LTP) or trajectory of each sounding and the measurements positions at a fixed height zo and time to and at displaced height dz and time dt. The steps of the procedure are outlined.

In order to optimize the reliability of the results we set the following requirements for the quartets. To constraint phase difference uncertainties in the nearly simultaneous triple we avoid using pairs of RO that are less than 70 km and more than 15 min apart (Schmidt et al., 2016). The fourth RO will have the same spatial requirement but to ensure that it will be able to sense the GW time evolution we require that the time difference with the remaining three ROs has to be at least 1 hr. To reduce the probability that not all the four profiles are sampling the same GW, we limit the separations between pairs to 300 km and 120 min. The line of sight (LOS) among all four retrievals must in addition differ by less than 10° to ensure that the atmosphere is being sampled in all of them in a similar way. In general, the requested conditions for triples have become more severe in studies over time (see, e.g., Faber et al., 2013; Hindley et al., 2015; Schmidt et al., 2016; Wang & Alexander, 2010). M. J. Alexander (2015) studied GW MF with triples from combined RO and High Resolution Dynamics Limb Sounder data and found that 10 to 20 min and 200 to 600 km sampling ranges produced variations around 20%.

The calculation of GW phase differences at given positions and times of the profiles has been performed by wavelet coherence (Torrence & Compo, 1998). It was applied at constant height to two neighboring T' profiles (equations (3)–(5)) or at two positions in one profile (equation (6)). Initially, we assumed that the phase difference $d\phi$ was between $-\pi$ and π; otherwise, we would have aliasing problems (e.g., Ern et al., 2004; Schmidt et al., 2016). However, we then also contemplated a possible "aliased $d\phi$" between -2π and 2π, that is, "$d\phi$" = $d\phi$ +/− 2π (depending whether $d\phi$ </> 0). Physically, this implies that we consider a priori one potential solution for each phase progression direction. If we assumed that the four phase differences at every height have no aliasing effect, then we could uniquely determine the solution (without sign uncertainty and therefore no propagation ambiguity). However, we include the possibility that we have detected an aliased $d\phi$, which as defined above will have opposite sign to the nonaliased one. We could consider more possible aliased cases, but this would lead to n^4 instead of 2^4 possible solutions. The above equation system then turns into 16 possible branches. Once we obtain the 16 solution sets of frequency and wave numbers ω, k, l, m (wavelengths $\lambda_x, \lambda_y, \lambda_z$), we remove from them any part where the phase difference approaches

and then exceeds $\pm 2\pi$ because it would imply that it surpasses one wave cycle. As we detect the phase differences in $[-2\pi, 2\pi]$ instead of $[-\pi, \pi]$, notice that the Nyquist requirements for acceptable (horizontal and vertical) wavelengths and period become halved.

Some physical constraints are then also imposed, which may further downsize from 16 the amount of acceptable solutions. (a) For the total horizontal wavelength λ_h, 100 km $< \lambda_h < \lambda_{h_c}$ so that it remains visible for RO (as stated above) and λ_{h_c} is defined to ensure that no GW frequency stays below or close to the inertial frequency (e.g., Schmidt et al., 2016). Also, λ_h must be larger than the (halved) Nyquist wavelength, which is here taken as the largest distance between all profile pairs at each height. (b) In the vertical direction 1.4 km $< \mid \lambda_z \mid <$ 20 km, where the limits are related to the (halved) Nyquist condition and the complete data height range. (c) The period must be less than the inertial period to ensure the midfrequency GW range (for valid use of the MF equation below) and stay above the largest time difference between all the RO pairs due to the (halved) Nyquist requirement. Thereafter, we also eliminate a solution if it exhibits an abrupt change of sign in any phase velocity component at any height. Also, any solution that does not have at least a valid 10 km height interval is discarded. After all these steps we may still have many different possible solutions. In order to eliminate the physically spurious options we introduce a root-mean-square (rms) procedure that assesses the fulfillment of the GW dispersion relation by every surviving solution. In the midfrequency range it is given by

$$\hat{\omega}^2 = \frac{N^2 \lambda_z^2}{\lambda_h^2} \tag{7}$$

where N is the Brunt-Väisälä frequency, which will be calculated from the RO T profiles. In order to obtain the intrinsic frequencies we need the horizontal components of wind, which were also obtained from ERA Interim reanalysis.

For the horizontal MF components calculations we use the following equations (see, e.g., Ern et al., 2004):

$$F_{x,y} = -\rho \frac{c_z}{c_{x,y}} \frac{1}{2} \left(\frac{g}{N}\right)^2 \left(\frac{To}{\bar{T}}\right)^2 \tag{8}$$

where g is gravity, ρ is density (obtainable from RO retrievals), and $\bar{T}$ stays for temperature background. We use the components of phase velocity c instead of the more usual wavelengths λ (without sign) in equation (8) as it preserves the adequate sign for $F_{x,y}$. RO typically underestimate GW amplitudes (P. Alexander, de la Torre, & Llamedo, 2008), which may lead to an equivalent effect in $F_{x,y}$ calculations according to equation (8).

3. Application Example

Only three sets emerged when the requirements on space, time, and LOS differences between the pairs of profiles within a quartet were applied to the whole RO database. Two quartets occurred on day 222 and another one on day 282 of the year 2006. As explained in general above, we proceed the following way. First, the background is removed from the four RO T profiles by the use of the Era Interim data. Thereafter, phase differences are calculated at every altitude z_1 for profiles 2, 3, and 4 with respect to 1 and for profile 1 between heights z_1 and z_1^*. Then, we are able to solve the four linear equations system (3)–(6) at every altitude z_1 to obtain the four unknowns k, l, m, ω at those heights. However, only one of the three quartets had at least one acceptable case after the above requirements on the solutions (frequency and wavelength ranges, a minimum 10 km height interval, and no unphysical abrupt change of sign in any phase velocity component). We interpret that the two quartets that provided no solutions either contained no detectable GW or their properties stayed beyond the resolution window of the method.

In Figure 2 we show for the surviving quartet the T and T' profiles of the four RO used to determine GW characteristics. They all exhibit some general similarities regarding temperature ranges, tropopause characteristics, and oscillation patterns. It may be seen that according to their latitudes and longitudes all of the soundings are located within 300 km distance and that three of them are separated in time by a few minutes, whereas the remaining one is about 2 hr away. For this final quartet, from the 16 possible solutions, only four satisfied the above requirements. We used then an assessment of minimum rms to evaluate the accomplishment of a dimensionless version of dispersion relation (7) along the whole altitude range and so keep the most appropriate of the four branches. The physically more meaningful solution was then found after calculation for each case of rms $(N^2 \lambda_z^2 / (\lambda_h^2 \hat{\omega}^2) - 1)$. The results showed slight changes with respect to the use of the full

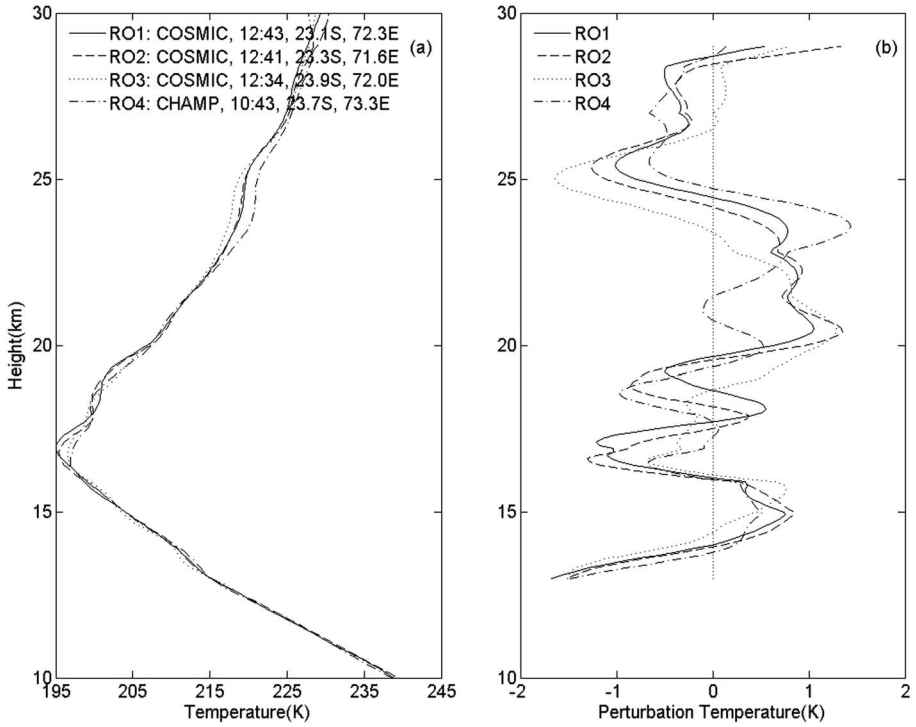

Figure 2. The four RO (a) T and (b) T' profiles on day 222 of year 2006 identified by mission, universal time, and location. CHAMP = CHAllenging Minisatellite Payload; COSMIC = Constellation Observing System for Meteorology, Ionosphere, and Climate; RO = radio occultation.

or the simplified midfrequency dispersion relation. Table 1 summarizes the tests of the physical constraints on the 16 solutions. The final choice of the most adequate of the four surviving cases by a minimum rms criterium is the one with the value 0.5. Notice that λ_z in the rms evaluation was not inferred from single profiles (apparent wavelength) but from the solution to the equation system (real value). As explained above, we finally checked for the final solution that all four RO were probably observing the same GW, which was done by comparing the mean dominant vertical wavelengths obtained when exchanging the RO used in equation (6). The results were respectively 3.9, 3.1, 3.4, and 3.2 km. The GW intrinsic period was also calculated with our solutions and the aid of the horizontal velocities provided by the ERA Interim reanalysis, and the average over the whole altitude range was about 11 hr (the inertial period at the latitude of our study was 30 hr).

Table 1
Rejection Causes in 12 of the 16 Solutions of the Analyzed Quartet in Terms of the Sign S_{ij} of the Four Phase Differences $d\phi_{ij}$: LH Stays for Horizontal Wavelength and TT for Period Out of the Accepted Range (Respectively 100 km $< \lambda_h < \lambda_{h_c}$ and Between the Inertial Period and the Nyquist Requirement)

$S_{21}S_{31}\backslash S_{41}S_{1*1}$	++	+−	−+	−−
++	0.8	2.6	TT, LH	TT, LH
+−	TT, LH	TT, LH	LH	LH
−+	1.0	0.5	TT, LH	TT, LH
−−	TT, LH	TT, LH	LH	LH

Note. In this quartet none of the solutions failed due to the conditions on the vertical wavelength, abrupt change of sign in phase velocity components, or a vertical profile smaller than 10 km. Dispersion relation root-mean-square values are indicated for the solutions satisfying the physical constraints.

In Figure 3 we show the calculated GW variables in terms of altitude according to the selected solution of the equation system for this quartet. Although the RO temperature information is provided between 10 and 30 km height, all calculated variables are shown below between 13 and 27 km as there are various intermediate quantities that require known values above and below every given vertical level (e.g., N and $d\phi$). We see the horizontal and vertical wavelengths, the horizontal phase speed c_h, the vertical phase velocity, the horizontal angle of phase propagation θ_P, the horizontal momentum magnitude F_h, and angle θ_F (180° out of phase with θ_P). The phase velocity components are given by

$$c_{x,y,z} = \frac{\omega}{k, l, m} \tag{9}$$

$$c_h = \left| \frac{\omega}{\sqrt{k^2 + l^2}} \right) \left| \tag{10}$$

whereby the signs of the k, l, m, ω solution must be carefully kept in order to adequately compute the phase velocity components (for example, if k, l, m, ω are all positive or all negative, it means phase progression toward east, north, and upward). Notice that it is not possible to find the horizontal

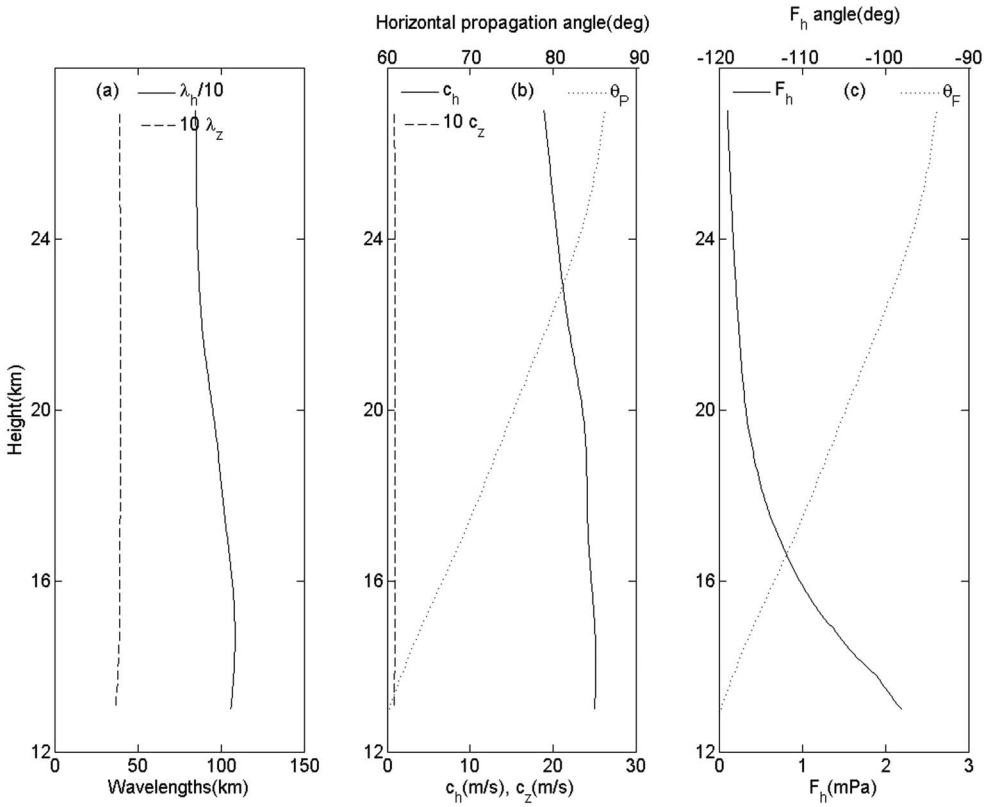

Figure 3. Gravity waves quantities against height obtained from the solution: (a) horizontal and vertical wavelengths; (b) horizontal phase speed as seen from the ground, vertical phase velocity, and horizontal phase propagation direction; c) absolute horizontal momentum and direction. The angles are measured counterclockwise from the East.

momentum flux angle unless one can determine univocally the horizontal wave propagation direction (see equation (8)). In Figure 3 wavelengths and phase velocity components remain nearly constant against height, momentum flux exhibits a sharp decrease, whereas the horizontal phase propagation and momentum flux directions show a 30° rotation in the studied altitude range. Depending on the RO used in equation (6), the mean vertical wavelength of our solution in the whole altitude range is located between 3.1 and 3.9 km (see above). The application of a wavelet analysis to each of the four RO temperature profiles against height leads respectively to the following values of one dominant vertical wavelength in each case: 6.5, 4.6, 5.1, and 5.1 km. As λ_z and MF have a linear relationship, the above calculated real values (3.1–3.9 km) imply that apparent values (4.6–6.5 km) may be producing an overestimation in both between 18% and 110%, which highlights the problem of using apparent rather than real wavelengths. In general, much worse outcomes could be expected (de la Torre et al., 2018). In our specific case, assuming a constant wave vector magnitude and angle and a straight sounding path, their formula provides an overestimation of λ_z and MF by 48% (sounding elevation angle 31° for RO1, angle of wave vector projected on the sounding plane 101°).

It is convenient to quantify the potentially achievable sample size of useful quartets in future missions. Combinations of GPS RO with other limb instruments have been contemplated in other works. We limit our estimations only to GPS RO quartets as the use of different instruments may lead to distortions in the calculations due to the different GW observational windows or heights that the diverse tools are able to see. If these combinations prove to be adequate in further works, then they will increase our estimations below of useful quartets in the future. Our study case above follows from extreme requirements that lead to optimal conditions for MF calculations. We now develop our estimation of useful quartets in future missions for more moderate requirements but which are not beyond the context of other recent works mentioned in the following lines. As stated above, M. J. Alexander (2015) found GW MF variations around 20 % for 10–20 min and 200 to 600 km sampling ranges. If we relax our requirements to both maximum values, increase the LOS variation maximum from 10° to 20°, and reduce the minimum distance between pairs from 70 to 50 km (Hindley et al., 2015 used respectively 30° and no minimum distance between pairs), we obtain 2,246 quartets.

However, 1,633 belong specifically to the six initial months of the COSMIC mission when all the satellites were close together. In our study only one out of three quartets was leading to a meaningful GW solution. If we consider the same proportion of one third of useful quartets, it would lead to an estimation of more than 250 GW MF values per month over the globe for the initial months of the COSMIC mission. On the other hand, we can use for our rough evaluation of useful quartets the estimations of McDonald (2012) on the percentage of paired profiles that are able to see the same GW in terms of distance and time separation. He found that approximately 50 % of the pairs at midlatitudes separated between 50 and 600 km and between 15 min and 2 hr (LOSs were mentioned as similar, but no value was given in that work) were seeing the same GW. In the case of independent observations the probability of observing the same GW would become 0.5^3 for any three pairs of RO profiles (e.g., 21, 31, and 41). However, they are not independent and our one third probability estimation (one useful quartet out three we had at disposal) for three dependent pairs looks as a reasonable intermediate value between one eighth and one half probability for just one pair (McDonald, 2012). Finally, a mission like COSMIC 2 would increase the amount of soundings from 2,000 to 12,000 per day. This would mean that more than 1,500 GW MF values over the globe per month could be obtained if a configuration similar to the initial months of COSMIC 1 was deployed.

4. Conclusions

With the expected future sharp increase of the space and time density of soundings (in particular GPS RO retrievals) this work presents a method that allows to exploit this potential in order to obtain net MF GW climatologies. This may be very valuable to improve climate simulations. In addition, the method allows to unambiguously determine in each analyzed case the direction of wave propagation and real wavelengths (as opposed to apparent ones detected in slant soundings). In our analyzed case we estimated that if real λ_z were not considered, there could have been an overestimation in this quantity and MF between 18% and 110%. The main method constraints and assumptions should be kept in mind when applying it: One dominant GW is observed by the four soundings, and it lies within the midfrequency and linear regime; GW and background are adequately separated by ERA Interim reanalysis, and there are no further aliasing effects than the considered one.

Acknowledgments
Manuscript prepared under grants CONICET PIP11220120100034, ANPCYT PICT 2013-1097, and German BMBF grant 01DN14001. P. Alexander and A. de la Torre are members of CONICET. GPS RO profiles were downloaded from cdaac-ftp.cosmic.ucar.edu and ERA Interim data from apps.ecmwf.int/datasets.

References

Alexander, M. J. (2015). Global and seasonal variations in three-dimensional gravity wave momentum flux from satellite limb-sounding temperatures. *Geophysical Research Letters*, *42*, 6860–6867. https://doi.org/10.1002/2015GL065234

Alexander, P., de la Torre, A., & Llamedo, P. (2008). Interpretation of gravity wave signatures in GPS radio occultations. *Journal of Geophysical Research*, *113*, D16117. https://doi.org/10.1029/2007JD009390

Alexander, P., de la Torre, A., Schmidt, T., Llamedo, P., & Hierro, R. (2015). Limb sounders tracking topographic gravity wave activity from the stratosphere to the ionosphere around midlatitude Andes. *Journal of Geophysical Research: Space Physics*, *120*, 9014–9022. https://doi.org/10.1002/2015JA021409

Alexander, M. J., Gille, J., Cavanaugh, C., Coffey, M., Craig, C., Eden, T., et al. (2008). Global estimates of gravity wave momentum flux from High Resolution Dynamics Limb Sounder observations. *Journal of Geophysical Research*, *113*, D15S18. https://doi.org/10.1029/2007JD008807

de la Torre, A., Alexander, P., Schmidt, T., Llamedo, P., & Hierro, R. (2018). On the distortions in calculated GW parameters during slanted atmospheric soundings. *Atmos Measurement Techniques*, *11*, 1363–1375. https://doi.org/10.5194/amt-11-1363-2018

de la Torre, A., Schmidt, T., & Wickert, J. (2006). A global analysis of wave potential energy in the lower stratosphere derived from 5 years of GPS radio occultation data with CHAMP. *Geophysical Research Letters*, *33*, L24809. https://doi.org/10.1029/2006GL027696

Ern, M., Hoffmann, L., & Preusse, P. (2017). Directional gravity wave momentum fluxes in the stratosphere derived from high-resolution AIRS temperature data. *Geophysical Research Letters*, *44*, 475–485. https://doi.org/10.1002/2016GL072007

Ern, M., Preusse, P., Alexander, M. J., & Warner, C. D. (2004). Absolute values of gravity wave momentum flux derived from satellite data. *Journal of Geophysical Research*, *109*, D20103. https://doi.org/10.1029/2004JD004752

Faber, A., Llamedo, P., Schmidt, T., de la Torre, A., & Wickert, J. (2013). On the determination of gravity wave momentum flux from GPS radio occultation data. *Atmos Measurement Techniques*, *6*, 3169–3180. https://doi.org/10.5194/amt-6-3169-2013

Geller, M. A., Alexander, M. J., Love, P. T., Bacmeister, J., Ern, M., Hertzog, A., et al. (2013). A comparison between gravity wave momentum fluxes in observations and climate models. *Journal of Climate*, *26*, 6383–6405. https://doi.org//10.1175/JCLI-D-12-00545.1

Healy, S. B., & Eyre, J. R. (2000). Retrieving temperature, water vapour and surface pressure information from refractive-index profiles derived by radio occultation: A simulation study. *Quarterly Journal of the Royal Meteorological Society*, *126*, 1661–1683.

Hindley, N. P., Wright, C. J., Smith, N. D., & Mitchell, N. J. (2015). The southern stratospheric gravity wave hot spot: Individual waves and their momentum fluxes measured by COSMIC GPS-RO. *Atmos Chemical Physics*, *15*, 7797–7818. https://doi.org/10.5194/acp-15-7797-2015

John, S. R., & Kumar, K. K. (2013). A discussion on the methods of extracting gravity wave perturbations from space-based measurements. *Geophysical Research Letters*, *40*, 2406–2410. https://doi.org/10.1002/grl.50451

Kursinski, E. R., Hajj, G. A., Schofield, J. T., Linfield, R. P., & Hardy, K. R. (1997). Observing Earth's atmosphere with radio occultation measurement using the Global Positioning System. *Journal of Geophysical Research*, *102*, 23,429–23,465.

Lange, M., & Jacobi, C. (2003). Analysis of gravity waves from radio occultation measurements. In C. Reigber, H. Lühr, & P. Schwintzer (Eds.), *First CHAMP Mission Results for Gravity, Magnetic and Atmospheric Studies* (pp. 479–484).

Luna, D., Alexander, P., & de la Torre, A. (2013). Evaluation of uncertainty in gravity wave potential energy calculations through GPS radio occultation measurements. *Advances in Space Research*, *52*, 879–882.

Marquardt, C., & Healy, S. (2005). Measurement noise and stratospheric gravity wave characteristics obtained from GPS occultation data. *Journal of the Meteorological Society of Japan*, *83*, 417–428.

McDonald, A. J. (2012). Gravity wave occurrence statistics derived from paired COSMIC/FORMOSAT3 observations. *Journal of Geophysical Research*, *117*, D15106. https://doi.org/10.1029/2011JD016715

Plougonven, R., & Zhang, F. (2014). Internal gravity waves from atmospheric jets and fronts. *Reviews of Geophysics*, *52*, 33–76. https://doi.org/10.1002/2012RG000419

Preusse, P., Dörnbrack, A., Eckermann, S. D., Riese, M., Schaeler, B., Bacmeister, J. T., et al. (2002). Space-based measurements of stratospheric mountain waves by CRISTA 1. Sensitivity, analysis method, and a case study. *Journal of Geophysical Research*, *107*, 8178. https://doi.org/10.1029/2001JD000699

Schmidt, T., Alexander, P., & de la Torre, A. (2016). Stratospheric gravity wave momentum flux from radio occultations. *Journal of Geophysical Research: Atmospheres*, *121*, 4443–4467. https://doi.org/10.1002/2015JD024135

Torrence, C., & Compo, G. P. (1998). A practical guide to wavelet analysis. *Bulletin of the American Meteorological Society*, *79*, 61–78.

Wang, L., & Alexander, M. J. (2010). Global estimates of gravity wave parameters from GPS radio occultation temperature data. *Journal of Geophysical Research*, *115*, D21122. https://doi.org/10.1029/2010JD013860

Wright, C. J., Hindley, N. P., & Mitchell, N. J. (2016). Combining AIRS and MLS observations for three-dimensional gravity wave measurement. *Geophysical Research Letters*, *43*, 884–893. https://doi.org/10.1002/2015GL067233

Wu, D. L., Preusse, P., Eckermann, S. D., Jiang, J. H., de la Torre Juarez, M., Coy, L., & Wang, D. Y. (2006). Remote sounding of atmospheric gravity waves with satellite limb and nadir techniques. *Advances in Space Research*, *37*, 2269–2277.